An integrated integral population model (IPM^2) to disentangle size-structured harvest and natural mortality

Abigail G. Keller[1,*], Benjamin R. Goldstein[2], Leah Skare[3], and Perry de Valpine[1]

[1]Department of Environment Science, Policy, and Management, University of California, Berkeley, Berkeley, California, USA

[2]Department of Forestry and Environmental Resources, North Carolina State University, Raleigh, NC, USA

[3]Northwest Straits Commission (ADD MORE)

[*]Corresponding author: Abigail G. Keller, agkeller@berkeley.edu

1 Abstract

2 Introduction

Assessing the efficacy of invasive species management interventions requires understanding if and how removal actions change population abundance and dynamics. However, population suppression can be challenging to differentiate from natural biological variation, reflecting the perennial challenge of distinguishing harvest and natural mortality in assessment of fishery stocks (Aanes et al., 2007). Often variability in harvest mortality is confounded with variability in natural mortality (Lewy & Nielsen, 2003), yet separating these fluctuations is crucial for obtaining reliable estimates of population abundance and demographic rates (Walters & Martell, 2004). Invasive species removal program success is highly variable (Prior et al., 2018), so reliably quantifying harvest rates and developing quantitative targets for suppression activities are essential for defining intervention success and efficiently allocating limited management resources (Green & Grosholz, 2021).

This challenge of disentangling sources of mortality is amplified for species with complex, size-structured demography. Body size can be one of the most important traits of an individual organism, often determining the strength of ecological interactions and influencing key life-history processes like growth and mortality (De Roos et al., 2003). The ontogenetic scaling of ecological performance with body size has been used to explain patterns at the population level (Werner, 1994). Population dynamics can be shaped by competitive

and predatory (cannibalistic) intra-specific interactions between different size cohorts (Claessen et al., 2004), predator-prey size-dependent functional responses (Aljetlawi et al., 2004), variable reproductive capacity across size (Hixon et al., 2014), and size-selective rates of harvest (Tu et al., 2018). Since these size-structured rates and interactions simultaneously modulate population dynamics, unraveling their individual contributions can be difficult.

Removal sampling data are the primary source of monitoring information for many invasive populations (Udell et al., 2022). While multinomial N-mixture models can be used to estimate abundance with animals removed successively from multiple sites (Dorazio et al., 2005), these models strictly assume population closure and no other sources of mortality. Additionally, invasive species datasets are often collected opportunistically as part of removal programs, rather than experimentally designed, limiting inference about population demographic rates (Crall et al., 2010; Rogosch & Olden, 2021; Tiberti et al., 2021). These removal observations are often not collected systematically across time and space and can be associated with large measurement error that can mask biological signals (Auger-Méthé et al., 2016; Katsanevakis et al., 2012; Sibert et al., 2003).

Despite the unique statistical inference challenges associated with invasive species removal data, the ecological, economic, and social costs of under- and over-estimating removal harvest rates can be high. Inefficient invasive population suppression plans can result in a waste of human and economic resources and can affect the confidence of people and stakeholders involved in removal (Tiberti et al., 2021). As invasive species management becomes more ambitious in scope and scale, population control can be controversial, stimulating conflicts among people and debates about achievability and efficiency (Crowley et al., 2017). These undesirable social outcomes underscore the need for rigorous assessments of the effectiveness of control programs.

Combining existing classes of models can be useful for distinguishing process and observation dynamics, facilitating parameter identifiability, and enabling inference of complex, size-structured demographic rates from imperfect observations. First, an integral projection model can be used to make population projections based on individual-level, size-dependent vital rates (Merow et al., 2014; Rees et al., 2014). In contrast to matrix population models with large data requirements, the integral projection model uses a kernel composed of continuous functions to describe the probability of transitioning between sizes due to size-dependent growth and mortality rates (Ellner & Rees, 2006). The integral projection model can therefore substantially simplify inference by only requiring estimates of parameters in these continuous functions, rather than parameters to describe every possible size transition.

The integral projection model can then be formulated in a state-space framework to estimate demographic rates with size-structured time series data (White et al., 2016). State-space approaches partition latent

process model dynamics from both process and measurement error, providing a hierarchical structure that separately models 1) an unobserved, process time series that reflects the true, hidden population state and 2) an observation time series that contains imperfect measurements related to the process time series (Auger-Méthé et al., 2021). By separating latent process model dynamics from both process and observation error, the state-space framework allows distinct estimation of harvest mortality — the observation process — from natural biological variation.

These state-space approaches, however, can suffer from challenges of parameter identifiability, especially in scenarios when information requirements of complex models exceed information available in a single dataset (Auger-Méthé et al., 2016). Integrated population models can resolve these identifiability issues by jointly analyzing multiple datasets in an integrated framework. By combining survey and demographic data, these models increase the precision of parameter estimates and facilitate estimation of "additional" parameters not identifiable with individual datasets (Abadi et al., 2010; Riecke et al., 2019). By combining an integrated population model with an integral projection model – an integrated integral projection model (IPM^2) – the relationship between individual traits and demographic performance can be used to forecast population-level processes (Plard et al., 2019).

An integrated integral projection model (IPM^2) will be useful for understanding size-structured population dynamics and removal effectiveness of invasive European green crab (*Carcinus maenas*). Listed as one of the world's 100 worst invaders (Lowe et al., 2000), the European green crab has successfully colonized all continents except Antarctica (Yamada, 2001), negatively impacting benthic communities (E. D. Grosholz, 2005), eelgrass habitat (Garbary et al., 2014; Howard et al., 2019), and commercial shellfish industries (E. Grosholz et al., 2011). The European green crab is a resilient marine invader, largely because of a mismatch in spatial scale between local removal programs and the crab's wide-ranging dispersal and population processes (Keller et al., 2025). While adult crabs occupy sheltered bays and estuaries, the crab's dispersal larval phase in open marine waters often facilitates recolonization of suppressed populations from neighboring habitats (Yamada et al., 2021). Understanding the relationship between removal effort and population suppression will therefore be critical for identifying the feasibility of suppression and for efficiently allocating conservation resources.

The green crab's local dynamics are regulated by complex, size-structured demography. Adult crabs exert direct control of recruitment, largely through strong negative adult-juvenile interactions (i.e., cannibalism) (E. Grosholz et al., 2021; Romano & Zeng, 2017). Competition with native crabs is also size-structured, with larger crabs maintaining a competitive advantage for space and resources (Jensen et al., 2007; McDonald et al., 2001). Importantly, these individual, size-structured interactions modulate population-level processes; a field experiment in California, USA found a 30-fold, single-year increase in total green crab abundance

in response to removal (E. Grosholz et al., 2021). This high level of juvenile survival associated with low adult abundance, often referred to as overcompensation or the "hydra effect", underscores the importance of quantifying size-structured population response to removal (Abrams 2009).

The green crab observation process is also size-selective, further complicating distinction between simultaneous size-structured processes. Common in marine systems, many green crab size classes are completely unobserved, as baited traps used for removal do not catch all individuals with equal probability across size classes (Jørgensen et al., 2009). Additionally, the observability of the population changes within a trapping season as individuals grow into size classes capable of being caught in traps. Quantifying the relationship between removal effort and size-structured removal rates will be necessary for assessing the feasibility and impact of removal, understanding long-term dynamics, and optimizing management actions and decisions for this high priority species.

Here we develop an integrated integral projection model (IPM^2) to quantify size-structured harvest rates of invasive European green crab. As part of a state-space framework, process dynamics are described using an integral projection model, where the population structure changes over time through seasonal growth, natural mortality, and removal, and observations are generated through the use of multiple size-selective removal methods (Figure 1). Combining multiple datasets in an integrated framework allows for distinct inference about size-structured harvest and natural mortality rates, "additional parameters" for which no explicit data is collected (Figure 2). The IPM^2 facilitates prediction of the stable size distribution and equilibrium abundance under different removal strategies, providing a framework for accurate assessment of the effectiveness of invasive species control programs.

3 Methods and materials

3.1 Demographic data

Population-level inference is focused on size-structured green crab abundance at Drayton Harbor in Washington, USA (Appendix 1.1, Figure A1.1). Data were collected from 2020-2023, with an intra-annual time series of size-structured removal count observations (D1, Figure 1B). Multiple trap types (Fukui, Minnow, and Shrimp) with different size-selective removal rates were used (Figure 1B), and traps were baited and left to "soak" in intertidal and subtidal habitat for 24-48 hours. Drayton Harbor is an enclosed bay, and we assume no movement in and out of the study site within each year.

Inference was supplemented by two additional datasets, size-at-age data (D2) and batch mark-recapture data (D3). Size-at-age data (D2) were collected from two sources: 1) records from crab removal observations

in northeastern Pacific estuaries from Yamada et al. 2005, when the somatic growth of a strong recruitment class was tracked over time, and 2) crabs with an assigned age from Drayton Harbor that were easily identifiable based on size and carapace color (Yamada et al., 2005). While data from these Drayton Harbor recruits entered the integrated population model likelihood twice (D1 and D2), extensive simulation-based research has revealed that IPMs are robust to dependent data (Abadi et al., 2010). Size-structured batch mark-recapture data (D3) was collected by Grosholz et al. 2021 in a mark-recapture experiment in Seadrift lagoon, California, USA (E. Grosholz et al., 2021). Here, green crabs were captured, marked, and released with Fukui traps and then recaptured within a few weeks, and batch markings do not allow individual identification.

More information on all three datasets can be found in Appendix 1.

3.2 Model description

We start by detailing the overall state-space population model, including the process and observation sub-models (Figure 1). We then describe how the parameters of the model are informed by the different datasets. Description of all model parameters can be found in Table 1.

3.2.1 Process model

The process model describes how unobserved, latent states depend on past states (Auger-Méthé et al., 2021). The following process equations describe the initial adult population size and annual recruitment, as well as the growth and survival kernel that projects the population forward in time based on seasonal size-dependent growth and size-dependent natural survival (Rees et al., 2014). These equations describe how the population changes within a year (intra-annual change) and between years (inter-annual change) (Figure 1). The model tracks the state of the population in terms of its distribution of carapace sizes, $N_{t,i,y}$, which is the density function of individuals of size y during year i at time t.

Initial population density and annual recruitment

The initial size distribution, $N_{t=1,i=1,y}$, is a function of the abundance of adults at the first time period during the first year, λ^A, the mean initial adult size in millimeters, μ_y^A, and the standard deviation of initial adult size in millimeters, σ_y^A. f_L represents the log-normal probability density function.

$$N_{t=1,i=1,y} = f_L(y; \mu_y^A, \sigma_y^A) \times \lambda^A \tag{1}$$

Ovigerous females spawn in August-December (Klassen & Locke, 2007), and these planktonic larvae

exit estuarine habitat to develop in high salinity coastal waters alongside larvae produced by neighboring habitats. Advection then brings larvae back into the estuary during recruitment (Young & Elliott, 2019). Reproduction is therefore modeled as an annual event with open demography, where the annual abundance of recruits, λ_i^R, is independent of adult abundance and follows a normal distribution, truncated such that $\lambda_i^R > 0$

$$\lambda_i^R \sim Normal(\mu_\lambda^R, \sigma_\lambda^R) \tag{2}$$

The annual size distribution of recruits, $R_{i,y}$, is a function of the annual abundance of recruits, λ_i^R, the mean initial recruit size in millimeters, μ_y^R, and the standard deviation of initial recruit size in millimeters, σ_y^R. f represents the normal probability density function.

$$R_{i,y} = f(y; \mu_y^R, \sigma_y^R) \times \lambda^R \tag{3}$$

Most crabs will settle from their planktonic larval stage in January to April (Yamada et al., 2005). The recruits therefore enter the process model in mid-May, corresponding to $t = 6$, when it can be assumed $\mu_y^R > 0$, yet before they grow into an observable size (Figure 1B).

$$N_{t=6,i,y} = N_{t=6,i,y} + R_{i,y} \tag{4}$$

Integral projection model

The population density is then projected forward in time using an integral projection model (IPM). The IPM uses a continuous distribution over y, and the abundance of individuals is discretized using a small size interval Δy centered on size y. The total population size, $N_{i,t}$ is $\int_\Omega N_{i,t,y} dy$, where Ω represents all biologically feasible sizes.

A kernel, $K(y', y, T)$, describes the probability density of moving from size y to size y'. This kernel is time-dependent, where $T = [D(t), D(t+1)]$, a vector of calendar dates associated with t and $t+1$. $N_{t+1,i,y}$ is therefore a function of $N_{t,i,y}$, $K(y', y, T)$, and the removed crabs, $n_{t,i,y}^R$

$$N_{t+1,i,y} = \int_\Omega K(y', y, T)(N_{t,i,y} - n_{t,i,y}^R) dy \tag{5}$$

In contrast to matrix population models with discrete size bins and transition probabilities between each size pair (Caswell, 2001), the kernel is defined as a combination of functions that are continuous over size y. The kernel is the product of a growth kernel, $G(y', y, T)$, and size-dependent natural survival, $S(y)$:

$$K(y', y, T) = G(y', y, T) \times S(y) \tag{6}$$

Seasonal growth

Like many ectotherms, green crab growth is strongly seasonal, with the growth rate peaking in the summer due to seasonal variation in temperature, light, and food availability (Contreras et al., 2003; García-Berthou et al., 2012). We therefore use a seasonal growth model that modifies the traditional von Bertalanffy growth model proposed by Beverton and Holt (Beverton & Holt, 2012; Somers et al., 1988).

$$\mu^G_{y,T} = y + (y_\infty - y)(1 - exp(-k\Delta t - S_t + S_{t0})) \tag{7}$$

$$S_t = \frac{Ck}{2\pi} sin(2\pi(D(t+1) - t_s) \tag{8}$$

$$S_{t0} = \frac{Ck}{2\pi} sin(2\pi(D(t) - t_s) \tag{9}$$

where $\mu^G_{y,T}$ is the mean size at $t+1$, y_∞ is the asymptotic average size, k is a measure of the exponential rate of approach to the asymptotic size, C modulates the amplitude of the growth oscillations, and t_s is the time between the start of the calendar year and the start of the convex portion of the first sinusoidal growth oscillation (García-Berthou et al., 2012).

To account for variation in growth rate among individuals, $G(y', y, T)$ is described as:

$$G(y', y = x, T) = f(y'; \mu^G_{y=x,T}, \sigma^G) \tag{10}$$

Natural mortality

The rate of natural mortality decreases with size, as smaller crabs have lower intra- and inter-specific competitive abilities and are more susceptible to predation and cannibalism (E. Grosholz et al., 2021; Maszczyk & Brzezinski, 2018). Natural survival, S, is described as:

$$S(y)_i = exp(-\Delta t(\beta_i + \frac{\alpha}{y^2})) \tag{11}$$

where β is the intensity of size-independent natural mortality and α is the intensity of size-dependent natural mortality (Carlson et al., 2010). Here, process error enters the model as year-specific, size-independent natural mortality:

$$\beta_i \sim Gamma(\beta_\alpha, \beta_\theta) \tag{12}$$

Density-dependent overwinter mortality

To transition from year i to year $i+1$, the population density experiences seasonal growth and density- and size-dependent overwinter survival. The abundance of crabs surviving the winter, $N_{t=1,i+1,y}$, is drawn from a binomial distribution, where *size* is the abundance of crabs after seasonal growth and removal in the last time period, t_{max}, and p is the probability of overwinter survival, $S^o_{y,i}$. Here $T = [D(t = t_{max}), D(t = 1)]$.

$$N_{t=1,i+1,y} \sim Binomial(\int_\Omega G(y', y, T)(N_{t_{max},i,y} - n^R_{t_{max},i,y})dy, S^o_{y,i}) \tag{13}$$

Due to thermal stress and starvation, the intensity of overwinter mortality is likely stronger than other times of the year and plays an important role in population regulation through density-dependent control on population size (Henderson et al., 1988). Overwinter mortality is also size-selective; smaller animals tend to have lower energy reserves than larger animals and use reserves more rapidly due to the allometry of metabolic rate (Hurst, 2007). Probability of overwinter survival, S^o, is therefore modeled as a density-size interaction, such that the intensity of size-dependent overwinter mortality increases at higher population densities. $N^T_{t_{max},i}$ is the total abundance at site i at the onset of winter.

$$S^o(y, N^T_{t_{max},i}) = exp(-\frac{\alpha^o_i \times N^T_{t_{max},i}}{y^2}) \tag{14}$$

Process error enters as a year-specific strength of density- and size-dependent overwinter mortality.

$$\alpha^o_i \sim Gamma(\alpha^o_\alpha, \alpha^o_\theta) \tag{15}$$

3.2.2 Observation model

Conditional multinomial observation model

A conditional multinomial observation model is used to describe the data-generating process for the removal count data $n^C_{t,i,y,j}$, representing the number of crabs of size y, caught at time t, during year i, in trap j (Figure 1) (Kéry & Royle, 2015). Multiple traps are placed simultaneously at each time period, so this method breaks the observation model into two pieces: 1) a binomial with an unknown sample size, the total abundance of crabs, $N_{t,i,y}$, and 2) a multinomial conditioned on a known sample size, the total number of removed crabs across all traps in each time period, $n^R_{t,i,y}$.

The total number of removed crabs, $n^R_{t,i,y}$, follows a binomial distribution with the total abundance of crabs, $N_{t,i,y}$, and total capture probability, $p_{t,i,y}$.

$$n^R_{t,i,y} \sim Binomial(N_{t,i,y}, p_{t,i,y}) \tag{16}$$

The size-structured count of crabs in each trap, $n^C_{t,i,y,j}$, follows a multinomial-dirichlet mixture distribution where the probability of capture in trap j, $p^C_{t,j,i,y}$, is conditioned on being captured at all, $p_{t,i,y}$. Since the trap compositional data are overdispersed due to green crab aggregation and spatial behaviors, the dirichlet allows for greater variance in the count data than predicted by a multinomial distribution (Thorson et al., 2017). The observed conditional probability of capture, $p^C_{t,j,i,y}$, therefore varies from the mean conditional probability of capture, $\tilde{p}^C_{t,j,i,y}$. More information on the multinomial-dirichlet mixture can be found in Appendix 2.2.

$$n^C_{t,j,i,y}|n^R_{t,i,y} \sim Multinomial(n^R_{t,i,y}, p^C_{t,j,i,y}|\tilde{p}^C_{t,j,i,y}) Dirichlet(\tilde{p}^C_{t,j,i,y}|\alpha^D_{t,j,i,y}) \tag{17}$$

Size-selective hazard rates

Harvest mortality through trapping occurs in continuous time, described as a size-selective hazard rate, $H(y)$, representing the instantaneous intensity of capture (Ergon 2018). The shape and magnitude of this size-selective hazard rate varies among the three trap types used for removal: Fukui, Minnow, and Shrimp traps.

Both Fukui and Shrimp traps capture larger crabs at higher rates than smaller crabs. The hazard rates, $H_F(y)$ and $H_S(y)$, of these trap types are a logistic function of crab size:

$$H_F(y) = \frac{h^{max}_F}{1 + e^{-h^k_F(y - h^0_F)}} \tag{18}$$

$$H_S(y) = \frac{h^{max}_S}{1 + e^{-h^k_S(y - h^0_S)}} \tag{19}$$

The Minnow trap mesh size is smaller than the maximum crab size, so the size-selective hazard rate follows a bell-shaped curve (Jørgensen et al., 2009).

$$H_M(y) = h^{max}_M \times exp(\frac{y - h^A_M}{2h^\sigma_M}) \tag{20}$$

Each baited trap, j, is placed in the habitat for a short (∼24-48 hrs) time interval, $\Delta b_{t,i,j}$. The probability of surviving trap mortality, $S_{t,i,y}$, is the integrated hazard rate, summed across all traps set during the same

time period, $O_{t,i}$.

$$S_{t,i,y} = exp(-\sum_{j=1}^{O_{t,i}} H_{t,j,i,y}\Delta b_{t,i,j}) \tag{21}$$

The total capture probability, $p_{t,i,y}$, is described as the probability of not surviving the trapping time interval, $p_{t,i,y} = 1 - S_{t,i,y}$. The mean conditional probability of capture, $\tilde{p}^{C}_{t,j,i,y}$, is then $H_{t,j,i,y} / \sum_{j=1}^{O_{t,i}} H_{t,j,i,y}$.

Integrated population model

We combined the population data from three data sources to jointly estimate demographic parameters, observation parameters, and latent states (Figure 2; Table 1). The size-at-age data (D2) directly informed the seasonal growth parameters. Inference was conducted sequentially, such that the seasonal growth parameters were fit with the size-at-age records, and the summarized posteriors were used to develop prior distributions in the overall IPM. More information on model fitting with D2 can be found in Appendix 1.2.

The mark-recapture data (D3) primarily informed the observation parameters that describe the size-selective hazard rates of the Fukui trap type, although these data also informed components of the growth and natural mortality kernel (Table 1; Figure 2). Inference using the time series data (D1, Figure 1B) and mark-recapture data (D3) was performed simultaneously, with both datasets entering the likelihood as data, rather than priors. The state-space model was therefore augmented with the following equations to integrate the mark-recapture data (D3).

The number of marked and released crabs of size y, n^{mc}_{y}, at t^{mc}_{1} underwent seasonal growth and natural mortality to the next time period, t^{mc}_{2}.

$$n^{mc}_{y,t_2} = \int_{\Omega} K(y', y, T^{mc}) n^{mc}_{y,t_1} dy \tag{22}$$

The number of recaptured and marked crabs of size y at t^{mc}_{2}, m^{mc}_{y}, follows a binomial distribution:

$$m^{mc}_{y} \sim Binomial(n^{mc}_{y,t_2}, p^{mc}_{y}) \tag{23}$$

where p^{mc}_{y} is the total probability of capture based on the total number of Fukui traps set, O^{mc}, over the time period Δb^{mc}:

$$p^{mc}_{y} = 1 - exp(-\sum_{j=1}^{O^{mc}} \int H_F(y)\Delta b^{mc}) \tag{24}$$

3.3 Model fitting

We fitted the integrated population model in a Bayesian framework using NIMBLE v.1.2.1 (de Valpine et al., 2017). We used vague priors for all parameters, which are provided in Appendix 2.1. Parameters were estimated by running four Markov chain Monte Carlo (MCMC) chains of 100 000 iterations, thinned by a factor of 10. Of the remaining 10 000 samples, 2 000 were discarded as burn-in. We used visual inspection of the MCMC chains and the Brooks and Gelman diagnostic $\hat{R}$ to assess model convergence, and we found that all parameters had an $\hat{R} \leq 1.05$ (Brooks & Gelman, 1998). All analyses were conducted in R v.4.41 (R Core Team, 2024). Code for the entire model is provided in Appendix 3, and generic, modular code that closely follows the model description is provided in Appendix 4. Posterior summaries, as well as convergence diagnostics and trace plots of model parameters can be found in Appendix 5.

To assess model performance and robustness, we conducted both a model selection and a model checking procedure (Conn et al., 2018). For model selection, we evaluated multiple functional forms of overwinter mortality using Watanabe–Akaike information criterion (WAIC). The inter-annual population transitions (i.e., transition from year i to year $i + 1$) are largely described by density-dependent overwinter mortality. Since density dependence only enters the model during this process and is therefore likely influential for forecasting the stable size distribution, we compared multiple functional forms for size- and density-dependent overwinter mortality and used the formulation with the lowest WAIC in the final analysis (Eq. 15-16, Appendix 6.1).

To check the model, we calculated posterior predictive p-values using the deviance as an omnibus discrepancy function and proportion of zeros as a targeted discrepancy function to check for zero inflation of the count data (Appendix 6.2). We found that the model was an adequate representation of the data-generating process, with p-values of 0.92 for both the deviance and proportion of zeros discrepancy functions (Appendix 6.2; Figures A.6.1 and A6.2).

3.4 Population forecasts

To evaluate how a green crab population responds to varying removal efforts, we conducted stochastic forward simulations with posterior samples. We randomly drew 1000 posterior samples, and for each posterior sample, we generated an initial adult population size and projected the population forward 25 years, applying varying removal efforts for each set of 1000 simulations. These varying removal efforts included a total of 0, 28, 112, 560, 840, 1400, and 2800 annual Shrimp, Fukui, or Minnow traps, applied evenly over the trapping season of 14 biweeks (21 total sets of 1000 simulations; seven removal efforts x three trap types). Year-varying quantities, like recruit abundance, size-independent natural mortality, and size- and density-

dependent overwinter mortality were drawn stochastically each year in the forward simulations (Table 1). To ensure proper comparisons between removal effort and trap type combinations, the same set of year-varying stochastic draws for each posterior sample was consistent across the 21 simulation sets.

For each simulation, S, the size-structured abundance at the end each of year after overwinter mortality, $N^{S}_{1,i+1,y}$, was recorded (Figure 1A). Simulation outputs were summarized as the mean size-structured abundance at the end of years 6-25, as the first five years were discarded as burn-in to ensure the population reached an equilibrium.

4 Results

4.1 Estimating population-level quantities

The integrated population model estimated size-structured European green crab abundance at Drayton Harbor (D1) at the beginning of each year in 2020-2023 (Figure 3). As the invasion progressed from 2020 to later years in 2021-2023, the size structure of adults shifted toward larger crabs (Figure 3A). The overall adult crab abundance decreased from 335 (274-430 95% CrI) adults in 2020 to 250 (238-266 95% CrI), 154 (146-164 95% CrI), and 165 (154-183 95% CrI) in 2021-2023. The size distribution of adults in 2021-2023 is also bimodal, as the recruit age class that survived the winter (year one class) had not yet grown in size to match the sizes of crabs older than one year.

The abundance of recruits varied by multiple orders of magnitude across years, ranging from 528 (253-969 95% CrI) and 1105 (668-1669 95% CrI) in the strong recruitment years of 2020 and 2022, to 42 (29-58 95% CrI) and 54 (20-102 95% CrI) in the weak recruitment years of 2021 and 2023 (Figure 3B).

4.2 Distinguishing size-structured natural and harvest mortality

By combining information in multiple datasets, the integrated population model allowed for estimation of "additional" parameters – size-structured natural and harvest mortality – that were not identifiable with the component datasets (Riecke et al., 2019).

Removal rates were estimated for three trap types – Fukui, Shrimp, and Minnow – with different rates of removal and size-selectivities (Figure 4). Overall, Shrimp traps removed crabs at the highest rate, and Minnow traps were only effective at removing crabs in the 30-60 mm size range. All traps do not effectively remove crabs smaller than 30 mm, consistent with the completely unobserved small crab portion of the population (Figure 1B).

Overwinter natural survival rates were lower than natural survival rates at other periods of the year

(Figure 5), consistent with the expectation that overwinter mortality plays an important role in population regulation. Overwinter survival rates were also density-dependent and corresponded to the recruitment strength: in the winters between 2020 and 2021 and between 2022 and 2023 – two years with the highest recruitment rates – the overwinter survival rates were lower.

4.3 Population forecasts

Forward simulations with posterior samples were used to forecast the stable size distribution and equilibrium abundance under different levels of removal effort, and subsequently different levels of removal mortality (Figure 6; Figure S1). These simulations indicated that a low removal effort with Fukui and Minnow traps (Figure 6B-C) resulted in only marginal changes in the stable size distribution and equilibrium abundance relative to no removal effort (Figure 6A). Large adult crabs can be completely removed from the population with a high removal effort of Shrimp traps (Figure 6D), but this large crab removal shifts the stable size distribution toward smaller crabs, as the equilibrium abundance of smaller crabs increases relative to no removal effort (Figure 6; Figure S2).

5 Discussion

highlights the role of body size in population dynamics and response to removal; this is why we need complex models whose information needs outpace the limited information available in individual datasets; and why we need robust methods to integrate disparate data sources

green crabs are an open population; previous work has suggested that long-term suppression is impractical because the rate of recolonization is so high; since removal cannot eradicate an open population, and instead shifts the size-structure, future work needs to measure size-dependent impacts (presumably impacts on eelgrass and shellfish are a function of biomass, rather than abundance), which will be useful for integrating this into a decision making framework to find the removal effort, and subsuquently the stable population size, that minimizes impact on habitat and resources

inclusion of mark-recapture data made model identifiable; however these datasets were collected in different locations with different habitats and scales of abundance (i.e., mark-recapture dataset came from a lagoon with $\tilde{1}$00,000 crabs, which about two orders of magnitude greater than drayton harbor). These dynamics of these sites may be different (i.e., abundance-induced heterogeneity in capture rates, especially if the crabs are aggregating around traps). While there are previous simulation studies, future work should investigate how violation of the assumption that the dynamics underlying the datasets are equal, how this affects estimates of "additional quantities"

6 Tables

Table 1: Notation and biological meaning of data, latent states, and parameters. Category refers to the parameter categories designated in Figure 2: 1) Init is the size structure of initial population density and annual recruits, 2) Growth is seasonal growth, 2) N. mort is size-dependent and size-independent natural mortality in non-winter months, 3) O. mort is size- and density-dependent overwinter mortality, 4) F obs, M obs, and S obs correspond to the size-selective observation process for Fukui, Minnow, and Shrimp traps, respectively, and 5) Latent corresponds to the latent states in the state-space model (Figure 1).

Symbol	Description	Category
	Demographic parameters	
μ_y^A	Mean adult size in millimeters at $t = 1$ and $i = 1$.	Init
σ_y^A	Standard deviation of adult size in millimeters at $t = 1$ and $i = 1$.	Init
μ_y^R	Mean recruit size in millimeters upon entry into the process model at $t = 6$.	Init
σ_y^R	Standard deviation of recruit size in millimeters upon entry into the process model at $t = 6$.	Init
y_∞	Asymptotic average crab size (carapace width, in mm).	Growth
k	Exponential rate of approach to the asymptotic size.	Growth
C	Parameter modulating the amplitude of seasonal growth oscillations.	Growth
t_s	Time between the start of the calendar year and the start of the convex portion of the first sinusoidal growth oscillation.	Growth
σ^G	Standard deviation of somatic growth.	Growth
β_i	Intensity of size-independent natural mortality in year i (not in winter months).	N. mort
α	Intensity of size-dependent natural mortality (not in winter months).	N. mort
β_α	Shape parameter of gamma distribution of intensity of size-independent natural mortality (not in winter months).	N. mort

β_θ	Rate parameter of gamma distribution of of intensity of size-independent natural mortality (not in winter months).	N. mort
α_i^o	Intensity of overwinter density- and size-dependent natural mortality in year i.	O. mort
α_α^o	Shape parameter of gamma distribution of intensity of overwinter density- and size-dependent natural mortality.	O. mort
α_θ^o	Rate parameter of gamma distribution of overwinter intensity of density- and size-dependent natural mortality.	O. mort
Observation parameters		
h^{max}	Maximum harvest mortality hazard rate. Maximum rate is trap type-specific, such that h_F^{max}, h_M^{max}, and h_S^{max} correspond to Fukui, Minnow, and Shrimp traps, respectively.	F Obs, M Obs, S Obs
h^k	Steepness of change from the minimum to the maximum hazard rate for trap types with a logistic size-selective function, such that h_F^k and h_S^k correspond to Fukui and Shrimp traps, respectively.	F obs, S obs
h^0	Midpoint of change from the minimum to the maximum hazard rate for trap types with a logistic size-selective function, such that h_F^0 and h_S^0 correspond to Fukui and Shrimp traps, respectively.	F obs, S obs
h_M^A	Crab size associated with maximum hazard rate with Minnow traps.	M obs
h_M^σ	Width parameter in the Minnow size-selectivity hazard rate function.	M obs
α^D	Parameter that governs the mean and variance of the multinomial-dirichlet mixture distribution.	F obs, M Obs, S Obs
Population-level quantities		

$N_{t,i,y}$	Population density function of individuals of size y, during year i, at time t.	Latent
λ^A	Adult abundance at the first time period, $t = 1$, during the first year, $i = 1$.	Latent
λ_i^R	Recruit abundance in year i.	Latent
μ_λ^R	Mean recruit abundance.	Latent
σ_λ^R	Standard deviation of recruit abundance.	Latent
	Observational data	
$n_{t,i,y}^R$	Count of removed crabs during time t, in year i, of size y in the time-series dataset (D1).	-
$n_{t,j,i,y}^C$	Count of removed crabs in time t, in trap j, in year i, of size y in the time-series dataset (D1).	-
$O_{t,i}$	Number of observations (traps) in time t, in year i in the time-series dataset (D1).	-
$W_{a,i}$	Size of crabs of a, during year i in the size-at-age dataset (D2).	-
n_y^{mc}	Number of marked and released crabs of size y in the mark-recapture dataset (D3).	-
m_y^{mc}	Number of recaptured marked crabs of size y in the mark-recapture dataset (D3).	-
O^{mc}	Number of observations (Fukui traps) in the mark-recapture dataset (D3).	-

7 Figures

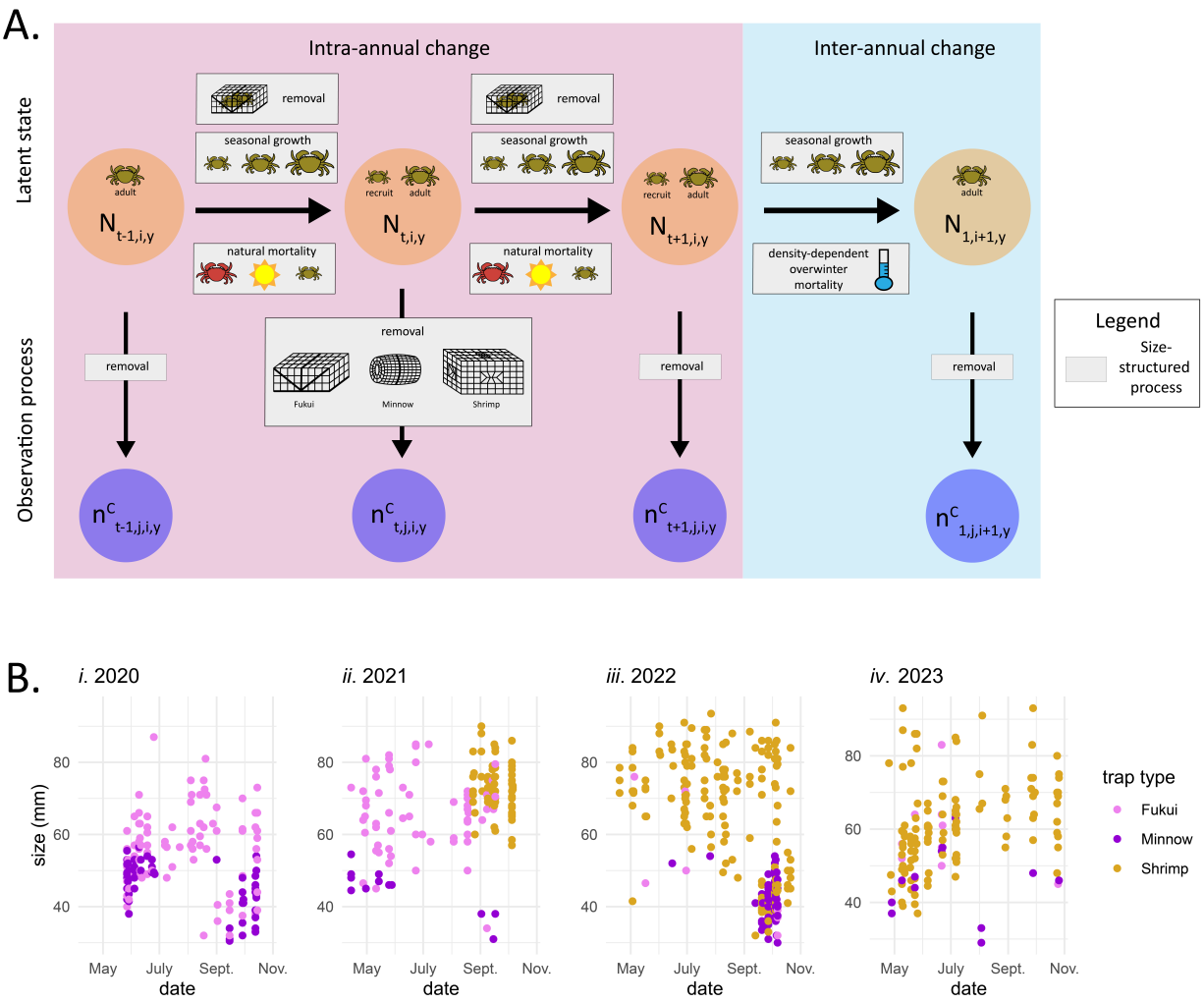

Figure 1: *A.* Conceptual diagram of state-space population model, including the dependence structure in the latent process dynamics and observation process. Orange circles designate the population density of individuals of size y during year i, at time t and are distinguished by dynamics within a year (intra-annual change) and dynamics between years (inter-annual change). Blue circles designate the count of removed crabs during time t, in trap j, in year i, of size y in the time-series dataset (D1). Grey boxes represent size-structured demographic and observation processes. *B.* Time series data (D1) collected in Drayton Harbor from 2020-2023, highlighting the relationship between time and crab size. Each point corresponds to one captured crab, and color corresponds to the type of trap used in capture.

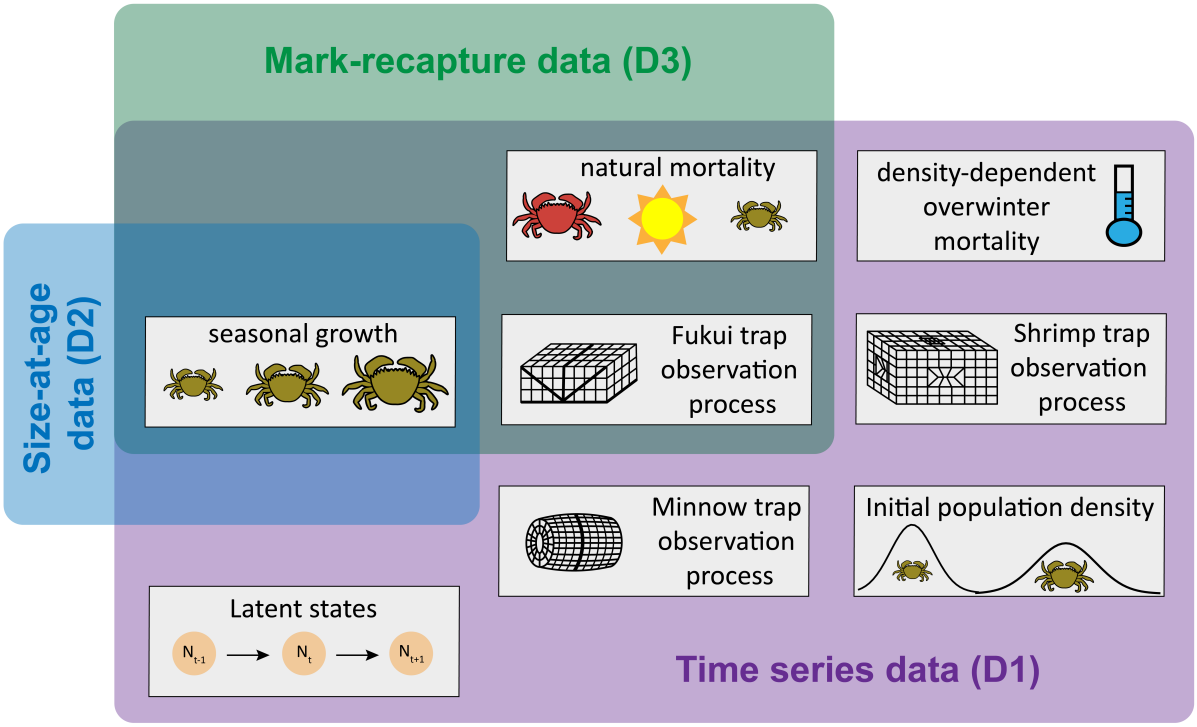

Figure 2: Overview of parameters informed by the three datasets in the integrated population model: time series data (D1) (Figure 1B), size-at-age data (D2) (Figure A1.1), and mark-recapture data (D3). Parameter categories correspond to categories designated in Table 1.

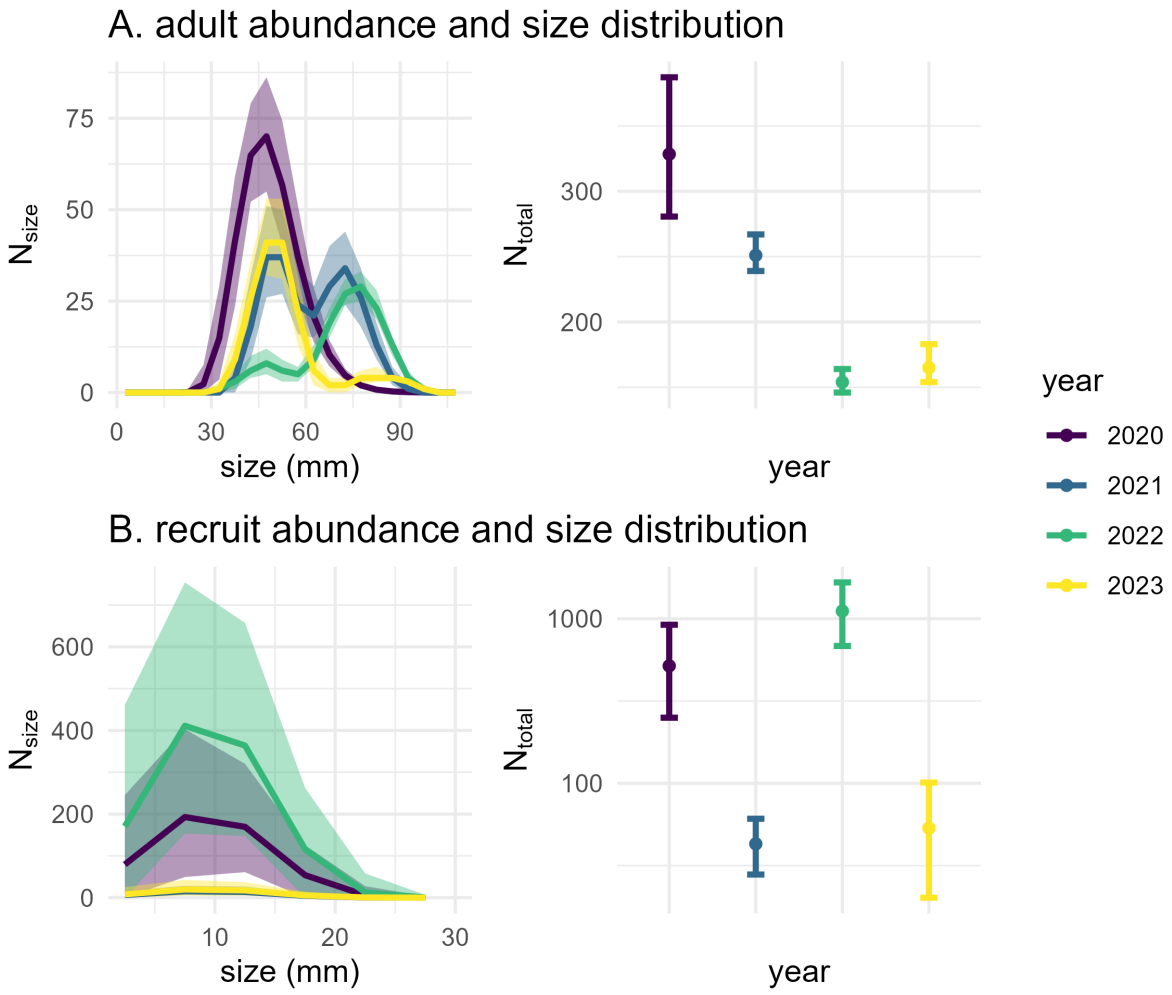

Figure 3: Total abundance and size distribution of *A.* adults and *B.* recruits. The left panels show the size distribution, or the number of individuals in each size class, N_{size}. The right panels show the total abundance of crabs across all size classes, N_{total}, in each year. Colors indicate the year, and error bars indicate the 95% credibility interval. Note that the right panel is the integral of the left panel.

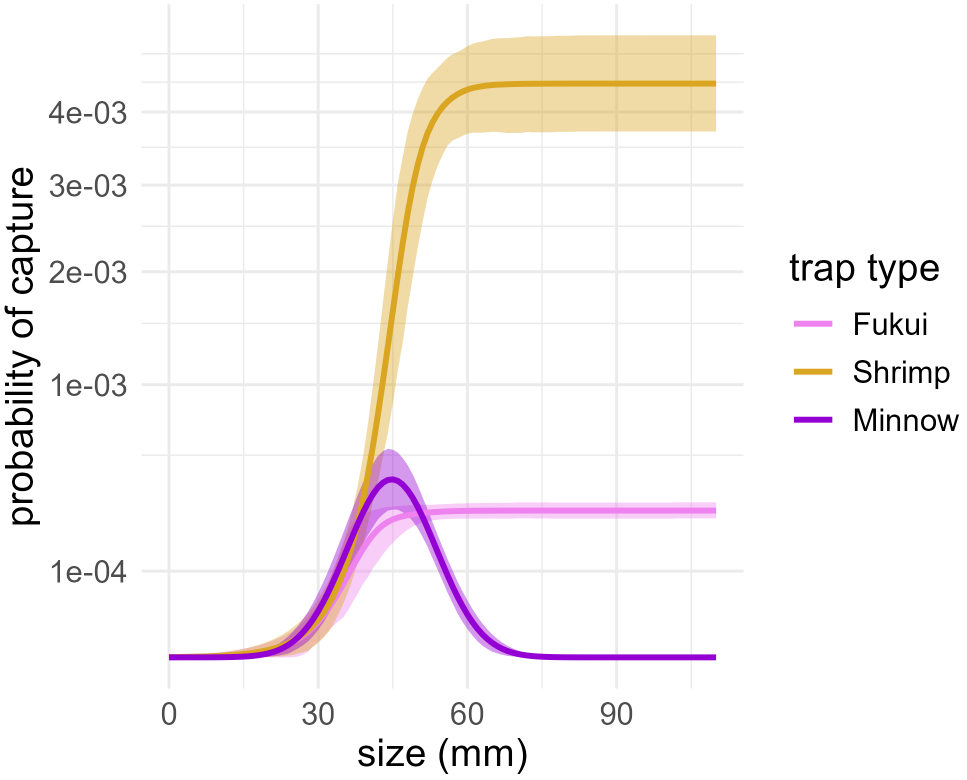

Figure 4: Size-structured probability of capture, p_y, in one trap over a 24 hours trapping period. Colors indicate the trap type. Note that the y-axis is presented with a square root transformation.

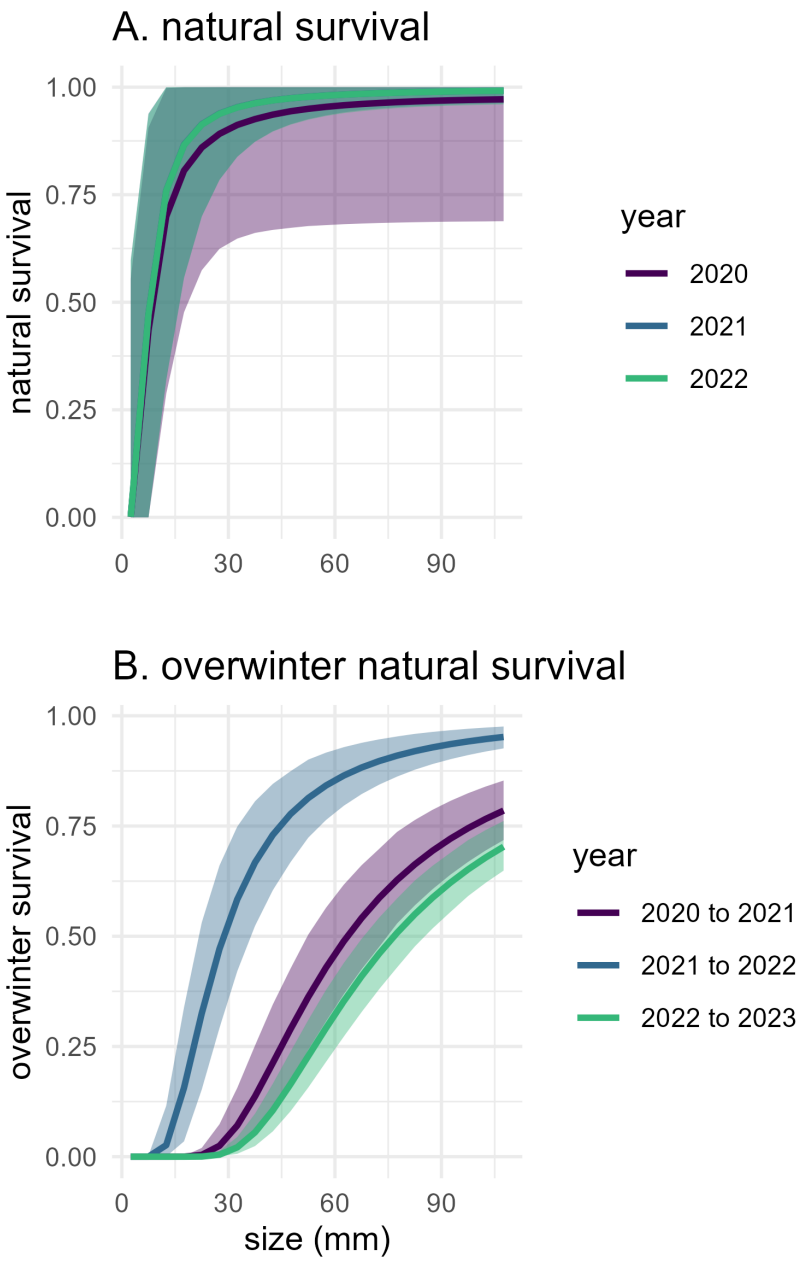

Figure 5: Size-structured natural survival rate in the *A.* non-winter season between Julian days 91 and 305 (Eq. 11) and *B.* overwinter (Eq. 15) between Julian day 306 and Julian day 90 of the following year. Colors indicate year, and error bars indicate the 95% credibility interval.

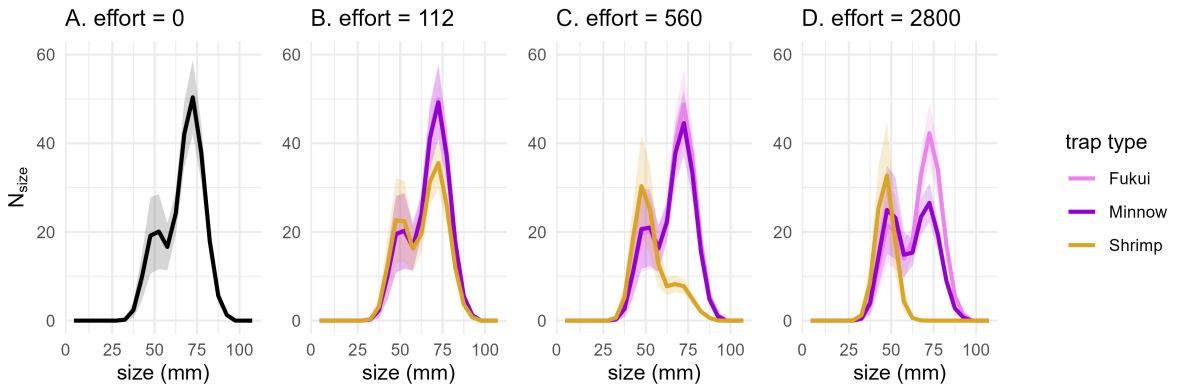

Figure 6: Population forecasts in response to varying removal efforts. Size distributions show the crab abundance in each size class, N_{size}, at the end of the year after overwinter mortality when *A.* 0 traps, *B.* 112 traps, *C.* 560 traps, and *D.* 2800 traps were applied evenly over a trapping season of 14 biweeks. Solid line indicates the median size-structured abundance across simulation replicates, and the shaded area indicates ± 1 standard deviation across simulation replicates. Colors indicate trap type used (i.e., in panel B, the purple line shows the resulting size distribution after a trapping effort of 112 Minnow traps).

References

Aanes, S., Engen, S., Sæther, B.-E., & Aanes, R. (2007). Estimation of the parameters of fish stock dynamics from catch-at-age data and indices of abundance: Can natural and fishing mortality be separated? *Canadian Journal of Fisheries and Aquatic Sciences*, *64*(8), 1130–1142.

Abadi, F., Gimenez, O., Arlettaz, R., & Schaub, M. (2010). An assessment of integrated population models: Bias, accuracy, and violation of the assumption of independence. *Ecology*, *91*(1), 7–14.

Aljetlawi, A. A., Sparrevik, E., & Leonardsson, K. (2004). Prey–predator size-dependent functional response: Derivation and rescaling to the real world. *Journal of Animal Ecology*, *73*(2), 239–252.

Auger-Méthé, M., Field, C., Albertsen, C. M., Derocher, A. E., Lewis, M. A., Jonsen, I. D., & Mills Flemming, J. (2016). State-space models' dirty little secrets: Even simple linear gaussian models can have estimation problems. *Scientific reports*, *6*(1), 26677.

Auger-Méthé, M., Newman, K., Cole, D., Empacher, F., Gryba, R., King, A. A., Leos-Barajas, V., Mills Flemming, J., Nielsen, A., Petris, G., et al. (2021). A guide to state–space modeling of ecological time series. *Ecological Monographs*, *91*(4), e01470.

Beverton, R. J., & Holt, S. J. (2012). *On the dynamics of exploited fish populations* (Vol. 11). Springer Science & Business Media.

Brooks, S. P., & Gelman, A. (1998). General methods for monitoring convergence of iterative simulations. *Journal of computational and graphical statistics*, *7*(4), 434–455.

Carlson, S. M., Kottas, A., & Mangel, M. (2010). Bayesian analysis of size-dependent overwinter mortality from size-frequency distributions. *Ecology*, *91*(4), 1016–1024.

Caswell, H. (2001). *Matrix population models: Construction, analysis, and interpretation. 2nd ed.* Sinauer Associates,Inc.

Claessen, D., De Roos, A. M., & Persson, L. (2004). Population dynamic theory of size–dependent cannibalism. *Proceedings of the Royal Society of London. Series B: Biological Sciences*, *271*(1537), 333–340.

Conn, P. B., Johnson, D. S., Williams, P. J., Melin, S. R., & Hooten, M. B. (2018). A guide to bayesian model checking for ecologists. *Ecological Monographs*, *88*(4), 526–542.

Contreras, H., Jaramillo, E., Duarte, C., & McLachlan, A. (2003). Population abundances, growth and natural mortality of the crustacean macroinfauna at two sand beach morphodynamic types in southern chile. *Revista Chilena de Historia Natural*, *76*(4), 543–561.

Crall, A. W., Newman, G. J., Jarnevich, C. S., Stohlgren, T. J., Waller, D. M., & Graham, J. (2010). Improving and integrating data on invasive species collected by citizen scientists. *Biological Invasions*, *12*, 3419–3428.

Crowley, S. L., Hinchliffe, S., & McDonald, R. A. (2017). Conflict in invasive species management. *Frontiers in Ecology and the Environment*, *15*(3), 133–141.

De Roos, A. M., Persson, L., & McCauley, E. (2003). The influence of size-dependent life-history traits on the structure and dynamics of populations and communities. *Ecology Letters*, *6*(5), 473–487.

de Valpine, P., Turek, D., Paciorek, C. J., Anderson-Bergman, C., Lang, D. T., & Bodik, R. (2017). Programming with models: Writing statistical algorithms for general model structures with nimble. *Journal of Computational and Graphical Statistics*, *26*(2), 403–413.

Dorazio, R. M., Jelks, H. L., & Jordan, F. (2005). Improving removal-based estimates of abundance by sampling a population of spatially distinct subpopulations. *Biometrics*, *61*(4), 1093–1101.

Ellner, S. P., & Rees, M. (2006). Integral projection models for species with complex demography. *The American Naturalist*, *167*(3), 410–428.

Garbary, D. J., Miller, A. G., Williams, J., & Seymour, N. R. (2014). Drastic decline of an extensive eelgrass bed in nova scotia due to the activity of the invasive green crab (carcinus maenas). *Marine biology*, *161*, 3–15.

García-Berthou, E., Carmona-Catot, G., Merciai, R., & Ogle, D. H. (2012). A technical note on seasonal growth models. *Reviews in Fish Biology and Fisheries*, *22*, 635–640.

Green, S. J., & Grosholz, E. D. (2021). Functional eradication as a framework for invasive species control. *Frontiers in Ecology and the Environment*, *19*(2), 98–107.

Grosholz, E., Ashton, G., Bradley, M., Brown, C., Ceballos-Osuna, L., Chang, A., de Rivera, C., Gonzalez, J., Heineke, M., Marraffini, M., et al. (2021). Stage-specific overcompensation, the hydra effect, and the failure to eradicate an invasive predator. *Proceedings of the National Academy of Sciences*, *118*(12), e2003955118.

Grosholz, E., Lovell, S., Besedin, E., & Katz, M. (2011). Modeling the impacts of the european green crab on commercial shellfisheries. *Ecological Applications*, *21*(3), 915–924.

Grosholz, E. D. (2005). Recent biological invasion may hasten invasional meltdown by accelerating historical introductions. *Proceedings of the National Academy of Sciences*, *102*(4), 1088–1091.

Henderson, P., Holmes, R., & Bamber, R. N. (1988). Size-selective overwintering mortality in the sand smelt, Atherina boyeri risso, and its role in population regulation. *Journal of fish biology*, *33*(2), 221–233.

Hixon, M. A., Johnson, D. W., & Sogard, S. M. (2014). Boffffs: On the importance of conserving old-growth age structure in fishery populations. *ICES Journal of Marine Science*, *71*(8), 2171–2185.

Howard, B. R., Francis, F. T., Côté, I. M., & Therriault, T. W. (2019). Habitat alteration by invasive european green crab (carcinus maenas) causes eelgrass loss in british columbia, canada. *Biological Invasions*, *21*(12), 3607–3618.

Hurst, T. (2007). Causes and consequences of winter mortality in fishes. *Journal of Fish Biology*, *71*(2), 315–345.

Jensen, G. C., McDonald, P. S., & Armstrong, D. A. (2007). Biotic resistance to green crab, carcinus maenas, in california bays. *Marine Biology*, *151*, 2231–2243.

Jørgensen, C., Ernande, B., & Fiksen, Ø. (2009). Size-selective fishing gear and life history evolution in the northeast arctic cod. *Evolutionary Applications*, *2*(3), 356–370.

Katsanevakis, S., Weber, A., Pipitone, C., Leopold, M., Cronin, M., Scheidat, M., Doyle, T. K., Buhl-Mortensen, L., Buhl-Mortensen, P., Anna, G., et al. (2012). Monitoring marine populations and communities: Methods dealing with imperfect detectability. *Aquatic Biology*, *16*(1), 31–52.

Keller, A. G., Counihan, T. D., Grosholz, E. D., & Boettiger, C. (2025). The transition from resistance to acceptance: Managing a marine invasive species in a changing world. *Journal of Applied Ecology*.

Kéry, M., & Royle, J. (2015). Modeling abundance using multinomial n-mixture models. *Applied hierarchical modeling in ecology, Kéry M, Royle JA, editors. Academic Press, Boston, Massachusetts*, 313–392.

Klassen, G. J., & Locke, A. (2007). *A biological synopsis of the european green crab, Carcinus maenas*. Citeseer.

Lewy, P., & Nielsen, A. (2003). Modelling stochastic fish stock dynamics using markov chain monte carlo. *ICES Journal of Marine Science*, *60*(4), 743–752.

Lowe, S., Browne, M., Boudjelas, S., De Poorter, M., et al. (2000). *100 of the world's worst invasive alien species: A selection from the global invasive species database* (Vol. 12). Invasive Species Specialist Group Auckland.

Maszczyk, P., & Brzezinski, T. (2018). Body size, maturation size, and growth rate of crustaceans. *The natural history of the Crustacea*, *5*, 35–65.

McDonald, P. S., Jensen, G. C., & Armstrong, D. A. (2001). The competitive and predatory impacts of the nonindigenous crab carcinus maenas (l.) on early benthic phase dungeness crab cancer magister dana. *Journal of Experimental Marine Biology and Ecology*, *258*(1), 39–54.

Merow, C., Dahlgren, J. P., Metcalf, C. J. E., Childs, D. Z., Evans, M. E., Jongejans, E., Record, S., Rees, M., Salguero-Gómez, R., & McMahon, S. M. (2014). Advancing population ecology with integral projection models: A practical guide. *Methods in Ecology and Evolution*, *5*(2), 99–110.

Plard, F., Turek, D., Grüebler, M. U., & Schaub, M. (2019). Ipm 2: Toward better understanding and forecasting of population dynamics. *Ecological Monographs*, *89*(3), e01364.

Prior, K. M., Adams, D. C., Klepzig, K. D., & Hulcr, J. (2018). When does invasive species removal lead to ecological recovery? implications for management success. *Biological Invasions*, *20*, 267–283.

R Core Team. (2024). *R: A language and environment for statistical computing*. R Foundation for Statistical Computing. Vienna, Austria. https://www.R-project.org/

Rees, M., Childs, D. Z., & Ellner, S. P. (2014). Building integral projection models: A user's guide. *Journal of Animal Ecology*, *83*(3), 528–545.

Riecke, T. V., Williams, P. J., Behnke, T. L., Gibson, D., Leach, A. G., Sedinger, B. S., Street, P. A., & Sedinger, J. S. (2019). Integrated population models: Model assumptions and inference. *Methods in Ecology and Evolution*, *10*(7), 1072–1082.

Rogosch, J. S., & Olden, J. D. (2021). Comparing opportunistic and strategic removal efforts to manage invasive fish species using a dynamic multi-state occupancy model. *Journal of Applied Ecology*, *58*(12), 2797–2809.

Romano, N., & Zeng, C. (2017). Cannibalism of decapod crustaceans and implications for their aquaculture: A review of its prevalence, influencing factors, and mitigating methods. *Reviews in Fisheries Science & Aquaculture*, *25*(1), 42–69.

Sibert, J. R., Musyl, M. K., & Brill, R. W. (2003). Horizontal movements of bigeye tuna (thunnus obesus) near hawaii determined by kalman filter analysis of archival tagging data. *Fisheries Oceanography*, *12*(3), 141–151.

Somers, I., et al. (1988). On a seasonally oscillating growth function. *Fishbyte*, *6*(1), 8–11.

458 Thorson, J. T., Johnson, K. F., Methot, R. D., & Taylor, I. G. (2017). Model-based estimates of effective sam-
459 ple size in stock assessment models using the dirichlet-multinomial distribution. *Fisheries Research*,
460 *192*, 84–93.
461 Tiberti, R., Buchaca, T., Boiano, D., Knapp, R. A., Pou Rovira, Q., Tavecchia, G., Ventura, M., & Tenan, S.
462 (2021). Alien fish eradication from high mountain lakes by multiple removal methods: Estimating
463 residual abundance and eradication probability in open populations. *Journal of Applied Ecology*,
464 *58*(5), 1055–1068.
465 Tu, C.-Y., Chen, K.-T., & Hsieh, C.-h. (2018). Fishing and temperature effects on the size structure of
466 exploited fish stocks. *Scientific reports*, *8*(1), 7132.
467 Udell, B., Martin, J., Waddle, H., Johnson, F., Falk, B., Yackel Adams, A., Funck, S., Ketterlin, J., Suarez,
468 E., Mazzotti, F., et al. (2022). Open removal models with temporary emigration and population
469 dynamics to inform invasive animal management. *Ecology and Evolution*, *12*(8), e9173.
470 Walters, C. J., & Martell, S. J. (2004). *Fisheries ecology and management*. Princeton University Press.
471 Werner, E. E. (1994). Ontogenetic scaling of competitive relations: Size-dependent effects and responses in
472 two anuran larvae. *Ecology*, *75*(1), 197–213.
473 White, J. W., Nickols, K. J., Malone, D., Carr, M. H., Starr, R. M., Cordoleani, F., Baskett, M. L., Hastings,
474 A., & Botsford, L. W. (2016). Fitting state-space integral projection models to size-structured time
475 series data to estimate unknown parameters. *Ecological Applications*, *26*(8), 2677–2694.
476 Yamada, S. B. (2001). *Global invader: The european green crab*. Oregon State University.
477 Yamada, S. B., Dumbauld, B. R., Kalin, A., Hunt, C. E., Figlar-Barnes, R., & Randall, A. (2005). Growth and
478 persistence of a recent invader *Carcinus maenas* in estuaries of the northeastern pacific. *Biological*
479 *Invasions*, *7*, 309–321.
480 Yamada, S. B., Gillespie, G. E., Thomson, R. E., & Norgard, T. C. (2021). Ocean indicators predict range
481 expansion of an introduced species: Invasion history of the european green crab carcinus maenas on
482 the north american pacific coast. *Journal of Shellfish Research*, *40*(2), 399–413.
483 Young, A. M., & Elliott, J. A. (2019). Life history and population dynamics of green crabs (*Carcinus maenas*).
484 *Fishes*, *5*(1), 4.